PHYSICAL REVIEW B **80**, 180506(R) (2009)

Transverse instabilities of multiple vortex chains in magnetically coupled $NbSe_2$/permalloy superconductor/ferromagnet bilayers

G. Karapetrov,[1,*] M. V. Milošević,[2] M. Iavarone,[1] J. Fedor,[1,3] A. Belkin,[1,4] V. Novosad,[1] and F. M. Peeters[2]
[1]*Materials Science Division, Argonne National Laboratory, Argonne, Illinois 60439, USA*
[2]*Departement Fysica, Universiteit Antwerpen, Groenenborgerlaan 171, B-2020 Antwerpen, Belgium*
[3]*Institute of Electrical Engineering, Slovak Academy of Sciences, Dubravska cesta 9, 841 04 Bratislava, Slovakia*
[4]*Physics Division, Illinois Institute of Technology, Chicago, Illinois 60616, USA*
(Received 8 September 2009; published 16 November 2009)

Using scanning tunneling microscopy and Ginzburg-Landau simulations, we explore vortex configurations in magnetically coupled $NbSe_2$/permalloy superconductor/ferromagnet bilayer. The permalloy film with stripe domain structure induces periodic local magnetic induction in the superconductor, creating a series of pinning-antipinning channels for externally added magnetic flux quanta. Such laterally confined Abrikosov vortices form *quasi-one-dimensional arrays* (chains). The transitions between multichain states occur through propagation of kinks at the intermediate fields. At high fields we show that the system becomes *nonlinear* due to a change in both the number of vortices and the confining potential. The longitudinal instabilities of the resulting vortex structures lead to vortices *"levitating" in the antipinning channels*.

DOI: 10.1103/PhysRevB.80.180506 PACS number(s): 74.78.Fk, 64.60.Cn, 74.25.Qt, 74.78.Na

Recently, much attention has been devoted to the studies of hybrid systems comprising of two or more elements with complementary physical properties, with the motivation that the resulting hybrid has a superior performance as compared to its constituents. Superconductor (S)/ferromagnet (F) hybrids exploit the interaction between the two "reservoirs" of strongly correlated electrons resulting in a wealth of new physical phenomena (for a review, see Ref. 1). The fundamental premise has been to isolate and tailor the dominant interaction between two correlated systems, as many overlapping interactions may conceal the discovery of new physical phenomena. Recent explorations focused solely on *magnetic interaction* between superconductor and ferromagnet have led to the discovery of numerous intriguing phenomena associated with magnetic pinning of Abrikosov vortices as well as with mesoscopic confinement of superconductivity.[2–8]

Confinement of superconductivity to quasi-one-dimension translates into confinement of the superconducting vortices. Abrikosov vortex structures constrained to one-dimensional (1D) superconducting condensate have been actively studied[9–15] in order to examine novel static and dynamic vortex phases. Magnetic imaging of the vortex structures in these systems have been challenging, in particular in the cases where the effective penetration depth of the superconductor (i.e., magnetic signature of the Abrikosov vortex) is on the order of the intervortex spacing. On the other hand, scanning tunneling microscopy (STM) can be successfully used to image the distribution of the *local order parameter* on the surface and map the Abrikosov vortex distribution in higher magnetic fields.

In this Rapid Communication, motivated by the aforementioned results, we study the vortex configurations in magnetically coupled superconductor $NbSe_2$/ferromagnet [permalloy (Py)] bilayer. We take advantage of well-ordered magnetic state of the Py film to induce 1D vortex confinement in the adjacent superconductor. We combine STM and Ginzburg-Landau (GL) simulations to explore the magnetic interaction between the magnetic domain state in a ferromagnet and Abrikosov vortices in an extreme type-II superconductor. $NbSe_2$ was chosen for its small coherence length (compared to the ferromagnetic domain size), negligible intrinsic pinning, and atomically flat and inert surface. The choice of thick Py film with well-ordered stripe domain pattern allows us to obtain a 1D periodic potential modulation of the superconducting condensate. Earlier we have shown that such a magnetic potential emanating from the ferromagnet can be used to achieve domain wall superconductivity.[8] Deeper in the superconducting state, strong interaction of the Abrikosov vortex lattice with the periodic magnetic domain structure leads to commensurability effects.[17]

The bilayer for the present study was prepared using the method elaborated in Ref. 16. 20-nm-thick SiO_2 insulating thin film was sputtered using rf magnetron on a freshly cleaved high-quality $NbSe_2$ single crystals [T_c=7.2 K, residual resistivity ratio (RRR)=40]. This layer was covered with a D=1-μm-thick Py ($Fe_{20}Ni_{80}$) overlayer using dc magnetron sputtering from a single target [Fig. 1(a)]. As-prepared sample was attached to a conducting substrate with the ferromagnetic layer down. The surface of $NbSe_2$ single crystal was cleaved successively until the color of the surface started to change. This is a first indication that the thickness of the $NbSe_2$ top layer is within the wavelength of the visible light. By further cleaving the sample the areas of different colors could be obtained, which signify different thicknesses of the superconductor.[18] The final thickness used in the STM studies in this work was approximately 0.4 μm and this value was verified by cross-sectional cut of the sample using focused ion beam milling and scanning electron microscopy metrology.

The thick Py film forms a narrow magnetic stripe domain pattern with a period comparable to the film thickness[19,20] [Fig. 1(b)]. The period of the domain structure W is proportional to the thickness D of the Py film. The magnetic stripe domain structure is insensitive to the magnetic field applied perpendicular to the film's surface up to 400 Oe, but forms

 ©2009 The American Physical Society

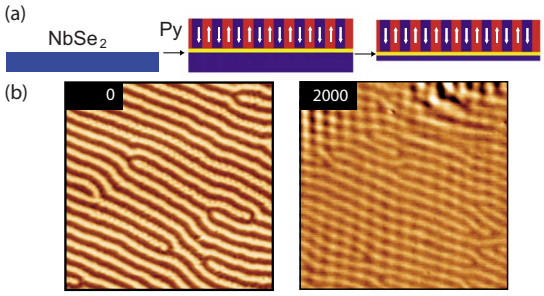

FIG. 1. (Color online) (a) Fabrication of magnetically coupled superconductor/ferromagnet structure: on a single crystal $NbSe_2$ a thin layer of insulating SiO_2 is evaporated followed by a 1-μm-thick permalloy. After cleaving the $NbSe_2$ down to submicron thickness, fresh atomically flat surface is exposed to the STM probe. (b) Magnetic force microscope images of the stripe domain pattern in Py at 0 and 2000 Oe applied field perpendicular to the surface of the film at room temperature. Scan area is 20×20 μm^2.

checkerboard domains in higher fields [Fig. 1(b)]. In our theoretical calculations, we used the dependence $W\approx 0.0109\sqrt{D}$ cm, following Ref. 21, and estimated magnetization of the film $M=1620$ G, exchange constant $A=2.665\times 10^{-6}$ erg/cm, and uniaxial anisotropy constant $K=2.63\times 10^{5}$ erg/cm^3.

The theoretical simulations of the described structure were performed within GL theory. We solve self-consistently a set of mean-field differential equations for the order parameter ψ and the vector potential $\mathbf{A}$,

$$(-i\nabla-\mathbf{A})^2\psi=(1-T-|\psi|^2)\psi, \tag{1}$$

$$-\kappa^2\nabla\times\nabla\times\mathbf{A}=\mathbf{j}. \tag{2}$$

The latter is the Maxwell-Ampere equation with a current density $\mathbf{j}=\Im(\psi^*\nabla\psi)-|\psi|^2\mathbf{A}$. The GL constant κ equals the ratio between the magnetic field penetration depth λ and the coherence length ξ and is in general very large for $NbSe_2$ samples. In the above expressions, all distances are expressed in units of $\xi(T=0)$, the vector potential in $\phi_0/2\pi\xi(0)$, and the order parameter in $\sqrt{-\alpha/\beta}$ with α,β being the GL coefficients. For more details on the numerics and implementation of periodic boundary conditions we refer to Ref. 22. Note that virial theorem requires integer number of flux quanta in the simulation region with periodic boundary, and we accommodate that by fixing the width of the simulation region to the period of magnetic domain structure W and the length is fitted (at $\approx 2W$) according to the applied magnetic field.

In STM measurements, the vortex images were obtained by spatially mapping the tunneling conductance value at the edge of superconducting energy gap at 4.2 K.[15] In Fig. 2, we show the local density of states map of 0.7×0.7 μm^2 area on $NbSe_2$ surface. Figure 2(a) shows a slightly distorted vortex chain at -100 Oe. The effective magnetic field above each domain is a sum of the contributions of the applied magnetic field and the field due to the local magnetization of Py. In the case when these two contributions are of the same

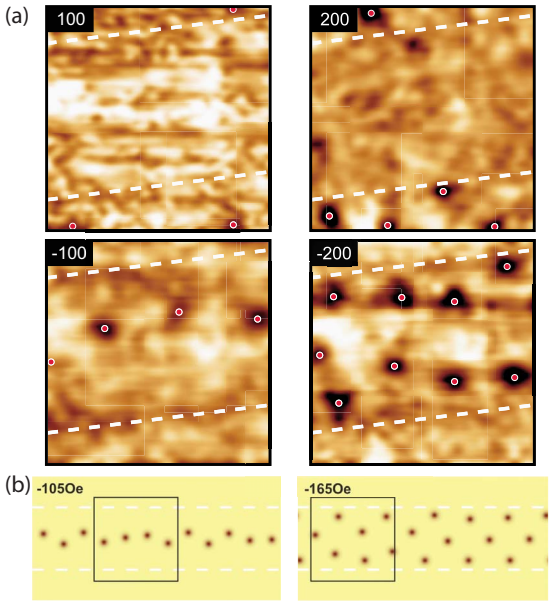

FIG. 2. (Color online) (a) STM images of vortex configurations in $NbSe_2$ at 4.2 K. Applied magnetic field values (in Oe) perpendicular to the surface of the superconductor are shown in the upper right corner. The white dotted lines show the underlying magnetic stripe domain boundaries. The scanning area is 0.7×0.7 μm^2. (b) Cooper-pair density plots, calculated at -105 and -165 Oe [in comparison with (a); see marked area], obtained for $D=1$ μm (plot sizes are 1.087×2.176 and 1.087×2.193 μm^2, respectively).

sign the effective fields are enhanced, and when they are of opposite sign the two contributions cancel each other. From our map it is obvious that the central part of the image is above a domain that has a "negative" polarity, i.e., the domain is collinear with the negative applied magnetic field. One expects that at 100 Oe the average vortex distance should be $a_v=\sqrt{(2/\sqrt{3})}\sqrt{(\Phi_0/B)}=0.489$ μm, and instead at -100 Oe the vortices form a quasi-1D chain state with an average distance of ≈ 0.210 μm. No vortices are observed at $+100$ Oe in the same area, being pinned at the adjacent domain.

Further increase in the negative applied field leads to an increase in the vortex density and formation of chain states similar to ones predicted in Ref. 9 and observed earlier in patterned superconducting $NbSe_2$.[15,23] The chains consist of periodically spaced vortices in the middle of the stripe domain. As the magnetic field increases so does the vortex density, leading to smaller intervortex spacing within a single chain. This process is continuous until a critical point leading to geometrical ordering transition and formation of double chains [Fig. 2(a) at -200 Oe] and triple chains [Fig. 3(a) at -300 Oe]. The similarities in vortex ordering and geometrical phase transitions with the case of a strong 1D confinement potential[9,15] end at this point. Further, with the help of simulations, we focus on the subtle but important effects that are specific to the nature of our confining potential.

We take advantage of the numerical simulations to reconstruct the vortex phase diagram of the magnetically coupled S/F bilayer system. Numerical solution of Eqs. (1) and (2) minimizes the Gibbs free energy of the sample, and Fig. 4

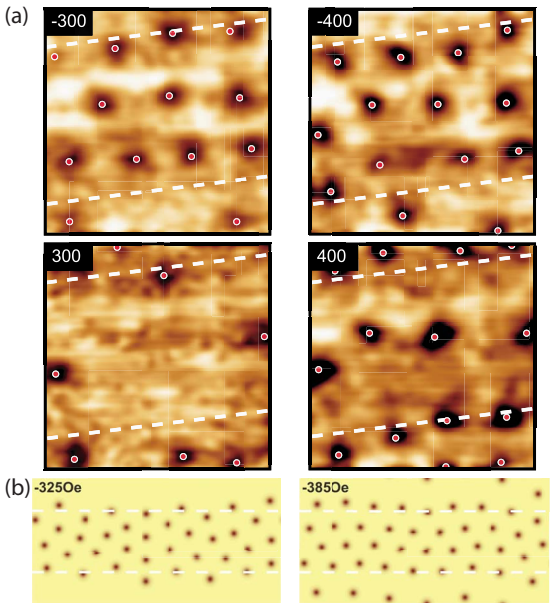

FIG. 3. (Color online) (a) Same as Fig. 2, but for $H=\pm 300$ and ± 400 Oe. (b) Cooper-pair density plots, calculated at -325 and -385 Oe, for $D=1$ μm (plot sizes are 1.087×2.176 and 1.087×2.193 μm^2, respectively).

shows the main outline of the ground-state phase diagram as a function of thickness of the Py film. Since this is a two-dimensional calculation, the stray field of the Py film has been averaged over given thickness of the $NbSe_2$ film, and as such put into Eqs. (1) and (2). The simulation region was $2W\times W$ large, and simulations were performed for $\xi(0)=10$ nm and $T=4.2$ K$\approx 0.6T_c$. The vortex states obey the imposed linear confinement and form *multiple vortex chains* (N of them) along the stripe domain with out-of-plane magnetization *parallel* to the applied field (as expected from the theory of magnetic pinning of vortices; see, e.g., Ref. 24). However, it should be emphasized that in reality transi-

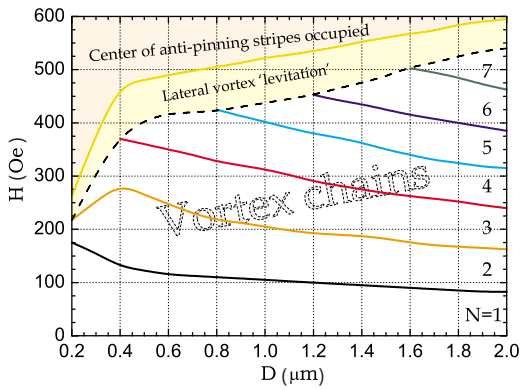

FIG. 4. (Color online) The equilibrium vortex phase diagram of the $NbSe_2$ film at $T=4.2$ K as a function of thickness of the underlying Py film D and external perpendicular field H (the domain structure of the Py film is assumed to be unperturbed by the applied field). N denotes the number of vortex chains along the positive magnetic domains [illustrated by $|\psi|^2$ contour plots on the right, dark (light) color—low (high) density]. At high fields, vortices penetrate areas above negative magnetic domains.

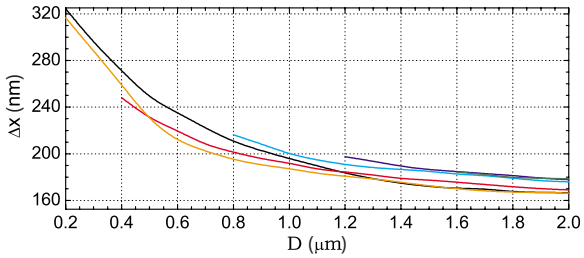

FIG. 5. (Color online) Average vortex spacing along the chain, prior to $N\rightarrow N+1$ chain configurational transition (color coding corresponding to Fig. 4), as a function of the thickness of the Py film.

tions between different N-chain states are not of first order. In increasing field, added vortex causes *local* chain instability by changing locally the transverse "optical" mode.[25] More instabilities eventually lead to a new ordered N-chain state via a so-called "zigzag"-type transition characteristic for quasi-1D Wigner crystals.[26] These transverse instabilities leading to different orderings are evident in Fig. 2, where the calculated vortex structures for the case of $D=1$ μm are given for $N=1\rightarrow 2$ and $N=2\rightarrow 3$ chain rearrangements, in comparison with experimentally obtained snapshots of vortex configurations.

Note however that vortex spacing Δx along the chain prior to the $N=2\rightarrow 3$ transition remains *larger* than $W/2(N+1)$, a value predicted for $N\rightarrow N+1$ transition in Ref. 9. In Fig. 5 we show the calculated vortex spacing along the chain prior to the formation of a new chain as a function of the thickness of the magnetic film (i.e., proportional to the domain width). The main conclusions following from Fig. 5 are that (i) the threshold vortex spacing decreases with the thickness of the magnetic film, but saturates for $D>1$ μm, and (ii) Δx is very weakly dependent on the number of chains N, contrary to findings of Ref. 9. Note that in quasi-1D confined classical systems, with hard-wall lateral boundaries, Δx also decreases with N (see, e.g., Ref. 27), while in our system lateral confinement is of parabolic type (where the decrease in Δx with N is slower[26]).

The discrepancy from the model[9] is caused by the nonrigid lateral confinement of the vortex chains. Namely, the superposition of the applied magnetic field and the stray field of the magnetic domains leads to slow expansion of the confinement potential for the superconducting vortices. From the magnetic force microscopy images at room temperature[8] and the STM maps in Fig. 2 we can reconstruct the position of the stripe domains under the $NbSe_2$ layer, and the domain boundaries are outlined with dashed lines in Figs. 2–4. However, beyond $N=3$ one notices that vortex chains may already occupy areas slightly beyond the domain boundaries. Therefore, with increasing magnetic field, not only that new vortices are added to the system, but the confinement potential is broadened as well. This leads to further lateral instability of the chains, in the areas of strongest interaction with effective confinement. Moreover, the attractive force acting on newly added vortices may gradually become *comparable* to the overall long-range interaction with earlier formed vortex chains, forcing the new vortices to reside in the antipinning channel above the magnetic domain of opposite polar-

ity. This is shown in Fig. 3, for fields ±300 Oe in experiment and 325 Oe in the simulation. Due to competing interactions, several vortices are levitating above the energetically nonfavorable domain. Beyond the field of 325 Oe in the simulations, we were unable to recover the linear chain state, unless we had the commensurate number of vortices in each chain. In every other case, the attempt of the large number of vortices to form an Abrikosov lattice in competition with linear confinement resulted in a sinusoidal-like modulation of the vortex structure, such as one shown in Fig. 3(b).

Further increase in the applied field leads to a larger number of vortices in the chains as well as above the antipinning domain. At certain conditions vortices at the antipinning channel may form a 1D structure, being equally repelled (on average) by chain structures from both adjacent domains. This is a very peculiar state since vortex *repulsion* in the antipinning domain is *strongest* in its central region. The existence of such a vortex ordering is verified in both theory (at ≈385 Oe) and experiment (at 400 Oe), as shown in Fig. 3. Beyond this field, vortices have little difficulty trespassing to the antipinning domain, which finally leads to a somewhat distorted Abrikosov lattice across the whole film.

To summarize, we studied the Abrikosov vortex configurations in magnetically coupled superconductor/ferromagnet bilayers. We elucidate the mechanism of quasi-1D topological vortex phase transitions in this system by theoretical simulations and STM vortex imaging. We demonstrate that transitions between 1D ordered vortex phases are accompanied by local transverse instabilities resulting in a local vortex disorder. This, in combination with magnetic-field-relaxed confinement, leads to lower threshold vortex densities for the geometrical transitions than in strongly confined systems such as superconducting stripes and hard-wall classical clusters. At higher magnetic fields the change in the number of vortices is accompanied with the change in the confinement potential resulting in nonlinear system response and vortex chain formation above the domains with opposite polarity. As a result, we found the "levitation" of vortices above the magnetic domains of opposite polarity, as well as vortex chain formation in this energetically unfavorable region, while the earlier formed chains are being sinusoidally distorted from the equilibrium Abrikosov vortex lattice.

This work as well as the use of the Center for Nanoscale Materials and the Electron Microscopy Center at Argonne National Laboratory was supported by UChicago Argonne, LLC, Operator of Argonne National Laboratory ("Argonne"). Argonne, a U.S. Department of Energy Office of Science laboratory, is operated under Contract No. DE-AC02-06CH11357. M.V.M. and F.M.P. acknowledge support from the Flemish Science Foundation (FWO-Vl), the Belgian Science Policy, the JSPS/ESF-NES program, the ESF-AQDJJ network, and the Vlaanderen-USA bilateral program.

*goran@anl.gov

[1] A. I. Buzdin, Rev. Mod. Phys. **77**, 935 (2005); I. F. Lyuksyutov and V. L. Pokrovsky, Adv. Phys. **54**, 67 (2005); F. S. Bergeret, A. F. Volkov, and K. B. Efetov, Rev. Mod. Phys. **77**, 1321 (2005); Y. A. Izyumov, Y. N. Proshin, and M. G. Husainov, Sov. Phys. Usp. **45**, 109 (2002); M. Velez, J. I. Martin, J. E. Villegas, A. Hoffmann, E. M. Gonzalez, J. L. Vicent, and I. K. Schuller, J. Magn. Magn. Mater. **320**, 2547 (2008).

[2] Z. Yang, M. Lange, A. Volodin, R. Szymczak, and V. V. Moshchalkov, Nature Mater. **3**, 793 (2004).

[3] L. N. Bulaevskii, E. M. Chudnovsky, and M. P. Maley, Appl. Phys. Lett. **76**, 2594 (2000).

[4] W. Gillijns, A. Y. Aladyshkin, M. Lange, M. J. Van Bael, and V. V. Moshchalkov, Phys. Rev. Lett. **95**, 227003 (2005).

[5] D. Stamopoulos, M. Pissas, and E. Manios, Phys. Rev. B **71**, 014522 (2005).

[6] M. V. Milošević and F. M. Peeters, Europhys. Lett. **70**, 670 (2005).

[7] V. V. Vlasko-Vlasov, U. Welp, G. Karapetrov, V. Novosad, D. Rosenmann, M. Iavarone, A. Belkin, and W. K. Kwok, Phys. Rev. B **77**, 134518 (2008).

[8] A. Belkin, V. Novosad, M. Iavarone, J. Fedor, J. E. Pearson, A. Petrean-Troncalli, and G. Karapetrov, Appl. Phys. Lett. **93**, 072510 (2008).

[9] S. H. Brongersma, E. Verweij, N. J. Koeman, D. G. de Groot, R. Griessen, and B. I. Ivlev, Phys. Rev. Lett. **71**, 2319 (1993).

[10] J. Guimpel, L. Civale, F. de la Cruz, J. M. Murduck, and I. K. Schuller, Phys. Rev. B **38**, 2342 (1988).

[11] M. O. Andre, M. Polichetti, H. Pastoriza, and P. H. Kes, Physica C **338**, 179 (2000).

[12] N. Kokubo, R. Besseling, V. M. Vinokur, and P. H. Kes, Phys. Rev. Lett. **88**, 247004 (2002).

[13] G. Stan, S. B. Field, and J. M. Martinis, Phys. Rev. Lett. **92**, 097003 (2004).

[14] I. V. Grigorieva, A. K. Geim, S. V. Dubonos, K. S. Novoselov, D. Y. Vodolazov, F. M. Peeters, P. H. Kes, and M. Hesselberth, Phys. Rev. Lett. **92**, 237001 (2004).

[15] G. Karapetrov, J. Fedor, M. Iavarone, D. Rosenmann, and W. K. Kwok, Phys. Rev. Lett. **95**, 167002 (2005).

[16] G. Karapetrov, J. Fedor, M. Iavarone, M. T. Marshall, and R. Divan, Appl. Phys. Lett. **87**, 162515 (2005).

[17] A. Belkin, V. Novosad, M. Iavarone, J. Pearson, and G. Karapetrov, Phys. Rev. B **77**, 180506(R) (2008).

[18] K. S. Novoselov, D. Jiang, F. Schedin, T. J. Booth, V. V. Khotkevich, S. V. Morozov, and A. K. Geim, Proc. Natl. Acad. Sci. U.S.A. **102**, 10451 (2005).

[19] N. Saito, H. Fujiwara, and Y. Sugita, J. Phys. Soc. Jpn. **19**, 1116 (1964).

[20] R. Spain, Appl. Phys. Lett. **3**, 208 (1963).

[21] R. Szymczak, J. Appl. Phys. **39**, 875 (1968).

[22] M. V. Milošević and F. M. Peeters, Phys. Rev. Lett. **93**, 267006 (2004).

[23] C. J. Olson Reichhardt, A. Libäl, and C. Reichhardt, Phys. Rev. B **73**, 184519 (2006).

[24] M. V. Milošević and F. M. Peeters, Phys. Rev. B **68**, 094510 (2003).

[25] B. Liu, K. Avinash, and J. Goree, Phys. Rev. Lett. **91**, 255003 (2003).

[26] G. Piacente, I. V. Schweigert, J. J. Betouras, and F. M. Peeters, Phys. Rev. B **69**, 045324 (2004).

[27] R. Haghgooie and P. S. Doyle, Phys. Rev. E **70**, 061408 (2004).